

Permanent Magnet Synchronous Generator for Offshore Wind Energy System Connected to Grid and Battery-Modeling and Control Strategies

Morlaye Sekou Camara^{*‡}, Mamadou Baïlo Camara^{*}, Brayima Dakyo^{*}, Hamid Gualous^{**}

^{*}Laboratoire GREAH - Université Le Havre, 75 rue Bellot, 76600 Le Havre –France

^{**}Laboratoire LUSAC-Université de Caen, Rue Louis Aragon, 50100 Cherbourg -Octeville, France

(camarasekou2012@gmail.com, camaram@univ-lehavre.fr, brayima.dakyo@univ-lehavre.fr, hamid.gualous@unicaen.fr)

[‡] Corresponding Author; Morlaye Sekou Camara, 75 rue Bellot, 76600 Le Havre –France, Tel: + 3302 32 85 99 00, camarasekou2012@gmail.com

Received: 24.12.2014 Accepted: 01.03.2015

Abstract- This paper describes modeling and control strategies of Permanent Magnet Synchronous Generators (PMSG) connected to lithium-ion battery pack to compensate intermittent energy from wind farm. Two PMSG and battery are connected to electrical grid through a back-to-back converter, and buck-boost converter in battery's side. Full system is connected to AC grid with phase to phase *RMS* voltage of 20kV. Proposed control strategies are focused on Maximum Power Point Tracking (MPPT) for PMSG speed control, active / reactive power, DC-bus voltage management and battery's power control. To show the control strategies performances, some simulation are done using Matlab / Simulink software.

Keywords- Active and reactive power control; AC/DC converter; DC/AC converter; DC/DC converter; DC-bus voltage control; Permanent Magnet Synchronous Generator (PMSG); Offshore wind energy management; Speed control; Maximum Power Point Tracking (MPPT).

1. Introduction

The industry of the wind generators has done a spectacular growth during these last years. Before, the wind generators power does not reach the order of megawatts. For this reason, the major part of the first models is based on Permanent Magnet Synchronous Generators or classical asynchronous generators. Conventional asynchronous generators are usually connected to turbine through a gear box. Permanent magnet synchronous generator (PMSG) can be coupled to turbine via a gear box or directly (without a gear box) if the generator has a high number of poles [1], [2].

Due to power increase in order of megawatts, until 10 MW today, PMSG configuration necessitates an increasing of the size and the weight of the converters. Compared to classical asynchronous generators, the permanent magnet synchronous generators have the advantages of being robust in construction, very compact in size, not requiring an additional power supply for magnetic field excitation, and requiring less maintenance. A variable speed wind energy conversion system including a PMSG offers advantages over the constant speed approach, such as maximum power point tracking capability and reduced acoustic noise at lower wind speeds [3-4]. An integration of energy storage devices in

wind turbines applications aims to answer the following problematic: - excess energy storage of the production compared to demand; - the supply of energy for the shortfall because of the intermittent behavior of wind.

In this paper, used energy storage device is based on lithium-ion battery which is considered to evaluate the proposed control strategies without any consideration for cost optimizing. In other terms, it is possible to use lower cost energy storage devices such as lead-acid battery, supercapacitors or flywheel with the same energy management strategies.

The contribution of this paper is focused on modeling and control strategies for wind farm production injection in electrical grid. System configuration is illustrated in Fig.1, where two generators are linked to electrical grid through a controlled converter which includes two three-phase rectifiers, a buck-boost converter, an intermediate DC-bus, and three-phase inverter, [5]. Full system is connected to AC grid of 20kV phase to phase *RMS* voltage.

Proposed control strategies include: Maximum Power Point Tracking (MPPT) for PMSG speed control, active/reactive power control, lithium-battery's power control and DC-bus voltage management.

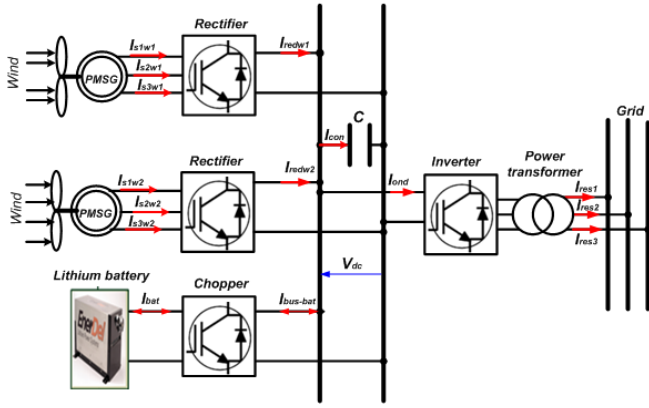


Fig.1. Wind farm configuration connected to lithium-battery.

To show the control strategies performances, some simulations are done using Matlab/Simulink software.

2. Wind Farm System Modeling

2.1. Wind turbine modeling

Theoretical power from a wind turbine is given in (1), where ρ is the density of air; S is the circular area swept by the turbine; β presents pitch angle, $V_{w1,w2}$ is the wind speed in [m/s], [6]. The ratio between the tip speed of the turbine and wind speed is expressed in (2), where Ω_m is the rotational speed of the turbine; R_t is the wind turbine radius.

$$P_t = \frac{1}{2} \cdot C_p(\lambda, \beta) \cdot \rho \cdot S \cdot V_{w1,w2}^3, S = 2 \cdot \pi \cdot R_t^2 \quad (1)$$

$$\lambda = \frac{\Omega_m \cdot R_t}{V_{w1,w2}} \quad (2)$$

The power coefficient C_p presents an aerodynamic output of the turbine limited to 0.593. This coefficient can be estimated using (3), [7]. Wind turbine mechanical torque C_m obtained from mechanical power is expressed in (4).

$$\begin{cases} C_p(\lambda, \beta) = (0.35 - 0.00167) \cdot (\beta - 2) \cdot \sin A \\ - 0.00184 \cdot (\lambda - 3) \cdot (\beta - 2) \\ A = \frac{\pi \cdot (\lambda + 0.1)}{14.34 - 0.3(\beta - 2)} \end{cases} \quad (3)$$

$$C_m = \frac{P_t}{\Omega_m} \quad (4)$$

The system dynamic equation can be expressed as presented in (5), where J_t and J_m present respectively the inertia moments of the turbine and the generator; f_v is the coefficient due to viscous rubbings of the generator; Ω_m is the generator rotational speed.

$$\begin{cases} (J_t + J_m) \cdot \frac{d}{dt}(\Omega_m) + f_v \cdot \Omega_m = C_m - C_{em} \\ J = (J_t + J_m) \end{cases} \quad (5)$$

2.2. PMSG modeling

PMSG dynamic model in dq axis can be writing as presented in (6), where R_s is the stator resistance, L_d and L_q are the inductances in stator, I_{sd} and I_{sq} present the currents in the stator; φ is the flux due to permanent magnet, p is the pair

of poles, [8].

$$\frac{d}{dt} \begin{bmatrix} I_{sd} \\ I_{sq} \end{bmatrix} = \begin{bmatrix} -\frac{R_s}{L_d} & \frac{p \cdot \Omega_m \cdot L_q}{L_d} \\ -\frac{p \cdot \Omega_m \cdot L_d}{L_q} & -\frac{R_s}{L_q} \end{bmatrix} \cdot \begin{bmatrix} I_{sd} \\ I_{sq} \end{bmatrix} + \begin{bmatrix} \frac{V_{sd}}{L_d} \\ \frac{V_{sq} - p \cdot \Omega_m \cdot \varphi}{L_q} \end{bmatrix} \quad (6)$$

In this paper, the smoothed poles permanent magnet synchronous generator is considered for system simulations which enables to write $L_d = L_q = L_s$.

2.3. Lithium-battery modeling

They are many electrical models in literature available to describe the electrochemical processes and dynamic behavior of the battery, such as the presented models in [9], [10], [11]. Used model in this paper is presented in Fig.2. This model includes an open circuit voltage E_{bat} which depends to State of Charge (SoC), internal resistances, a parallel RC circuit which describes the charge transfer and the diffusion process between the electrode and the electrolyte [12-13]. The analytical model of the lithium-battery pack is presented in (7), where R_Ω and R_C are respectively series and polarization resistances, C_c presents the parallel circuit capacitance, N_s and N_p are respectively the cells number in series and parallel.

$$\begin{cases} V_{bat} \approx N_s \cdot E_{bat} - \frac{N_s}{N_p} \cdot Z \cdot I_{bat} \\ \tau = C_c \cdot R_C \\ Z = R_\Omega + \frac{R_C}{1 + \tau \cdot s} \end{cases} \quad (7)$$

2.4. DC/DC converter modeling for battery pack

To develop the bidirectional converter model, the buck and boost operations must be analyzed, [14], [15], [16]. During buck converter mode, $K1$ semiconductor is switched ON, while $K2$ is OFF. Contrary to this mode, $K2$ is switched ON, while $K1$ became OFF. For this study, I_{bat} and $I_{bus-bat}$ are supposed negative during the battery's charge operations (buck converter mode), and they are positive during the battery discharge (boost converter mode). Average model of the converter presented in Fig.3 is given in (8), where, k and α can have the following values:

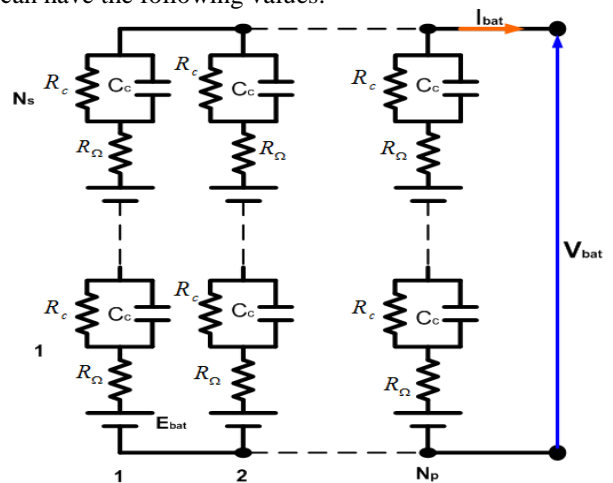


Fig.2. Lithium-battery model.

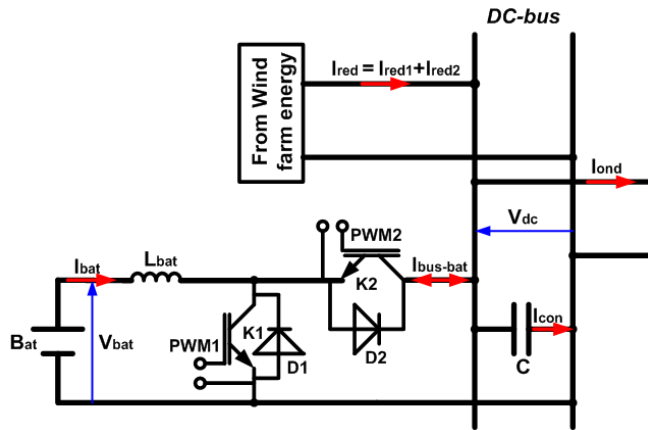


Fig.3. Lithium-battery connection configuration.

- In boost converter mode: $k = 1$ and $\alpha = 1 - \alpha_1$, where α_1 is the boost converter duty cycle average value.
- In buck converter mode: $k = -1$ and $\alpha = \alpha_2$, where α_2 is the buck converter duty cycle average value.

This model has a nonlinear behavior because of crosses between the control variables (α_1, α_2) and the state variables (I_{bat} and V_{dc}). The V_{bat} and I_{bat} variables are likely to disturb the control, they must be measured and used in the control loop to ensure a dynamic control.

$$\begin{cases} V_{Lbat} = L_{bat} \cdot \frac{d}{dt}(I_{bat}) = k \cdot (V_{bat} - \alpha \cdot V_{dc}) \\ I_{redw1} + I_{redw2} = I_{ond} + I_{con} + k \cdot I_{bus-bat} \end{cases} \quad (8)$$

2.5. AC/DC and DC/AC converters modelling

This section presents the analytical model of the controlled three phase's converters (rectifier and inverter). Based on Fig.1, the DC-bus currents enable to write the analytical model of rectifier presented in (9), where DC-bus capacitor C is assumed not charged. In this equation, I_{ond} presents the inverter input current; $I_{s1w1,w2}$, $I_{s2w1,w2}$ and $I_{s3w1,w2}$ correspond to rectifiers input currents; $I_{bus-bat}$ presents battery's contribution in DC-bus; S_a, S_b and S_c present the three phase pulse with modulation (PWM) signals applied to rectifiers.

$$\begin{cases} I_{redw1} = S_a \cdot I_{s1w1} + S_b \cdot I_{s2w1} + S_c \cdot I_{s3w1} \\ C \cdot \frac{d}{dt}(V_{dc}) = I_{redw1} + I_{redw2} - I_{ond} - k \cdot I_{bus-bat} \\ I_{redw2} = S_a \cdot I_{s1w2} + S_b \cdot I_{s2w2} + S_c \cdot I_{s3w2} \end{cases} \quad (9)$$

The three phase inverter output voltages can be estimated as expressed in (10), where V_{dc} is the DC-bus voltage, w_1, w_2 and w_3 present the three phase pulse with modulation (PWM) signals applied to inverter.

$$\begin{cases} V_{Sa} = \frac{2 \cdot w_1 - w_2 - w_3}{3} \cdot V_{dc} \\ V_{Sb} = \frac{2 \cdot w_2 - w_1 - w_3}{3} \cdot V_{dc} \\ V_{Sc} = \frac{2 \cdot w_3 - w_1 - w_2}{3} \cdot V_{dc} \end{cases} \quad (10)$$

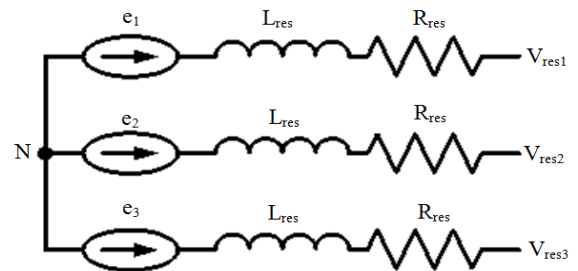


Fig.4. Model of electrical grid.

2.6. Electrical grid modeling

The main goal of this section consists to establish an ideal model of electrical grid. To establish this model, the balanced three phase system is considered. Considered model in this paper is presented in Fig.4, where V_{res1}, V_{res2} and V_{res3} voltage are connected to three phase inverter ($V_{sa,b,c}$) through a transformer with a ratio of m . Analytical model of electrical grid is presented in (11), where e_1, e_2 and e_3 present the conventional three phase *emf* with phase to phase RMS voltage of 20kV.

$$\begin{cases} V_{res1} - e_1 = R_{res} \cdot I_{res1} + L_{res} \cdot \frac{d}{dt}(I_{res1}) \\ V_{res2} - e_2 = R_{res} \cdot I_{res2} + L_{res} \cdot \frac{d}{dt}(I_{res2}) \\ V_{res3} - e_3 = R_{res} \cdot I_{res3} + L_{res} \cdot \frac{d}{dt}(I_{res3}) \end{cases} \quad (11)$$

3. Offshore Wind Energy System Control Strategies

The control strategies of the system include [17]: - The PMSG speed control based on Maximum Power Point Tracking (MPPT) technique. - The active and the reactive powers control using an inverter connected to grid. - DC-bus voltage control through two rectifiers connected to two permanent magnet synchronous generators.

3.1. PMSG speed control strategy

Speed references for two wind turbines are expressed in (12), where $v_{w1,w2}$ present the wind speed profiles for two wind turbines. These references are obtained from MPPT technique. The control strategy of the two PMSG speeds is illustrated in Fig.5.

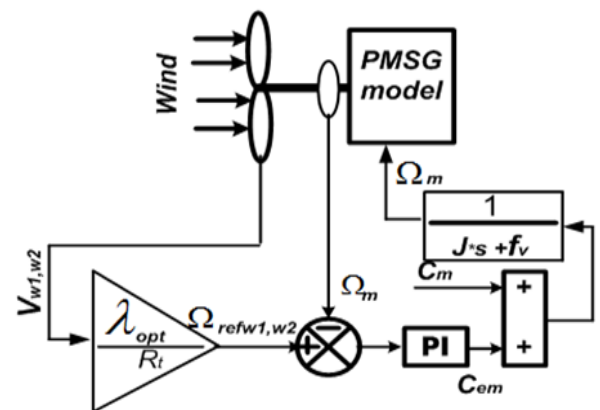


Fig.5. PMSG speed control loop for each wind turbine.

$$\Omega_{refw1,w2} = \frac{\lambda_{opt} \cdot v_{w1,w2}}{R_t} \quad (12)$$

The PI controller coefficients obtained from closed loop analysis are shown in (13), where ω_{nd} presents the dynamics of the system, and t_{sd} is the control loop time constant, [18].

$$\begin{cases} K_p = \sqrt{2} \cdot \omega_{nd} \cdot (J_t + J_m) \\ K_i = \omega_{nd}^2 \cdot (J_t + J_m) \end{cases}, \omega_{nd} = \frac{5.8}{t_{sd}} \quad (13)$$

3.2. Active and reactive power control

Active and reactive powers injected in electrical grid is expressed in (14), where (V_{dres}, V_{qres}) and (I_{dres}, I_{qres}) are respectively the voltage and current in dq axis.

$$\begin{cases} P_{wf} = V_{dres} \cdot I_{dres} + V_{qres} \cdot I_{qres} \\ Q_{wf} = V_{qres} \cdot I_{dres} - V_{dres} \cdot I_{qres} \end{cases} \quad (14)$$

The active and reactive power control strategies are presented in Fig.6. PI controllers coefficients used in inner and outer loops are respectively presented in (15).

$$\begin{cases} K_{pir} = \frac{2.197 \cdot L_{res}}{t_{ir}} \\ K_{iir} = \frac{2.197 \cdot R_{res}}{t_{ir}} \end{cases}; \begin{cases} K_{pp} = \frac{t_{ir}}{t_p} \\ K_{ip} = 2.197 \cdot t_p \end{cases} \quad (15)$$

3.3. Battery's power control strategy

Battery's power reference is estimated from difference between the available power P_{dis} and required power for electrical grid P_{ref} , as expressed in (16). If $P_{batref} \geq 0$ the boost converter is used, else if the buck converter is switched.

$$P_{batref} = P_{dis} - P_{ref} \quad (16)$$

Battery's power control strategy is presented in Fig.7, where bidirectional behavior of the buck-boost converter is due to sign of P_{batref} . The parameters of PI controller are presented in (17), where ω_{nb} and L_{bat} are respectively the dynamics of the system, and smoothing inductance of battery's current.

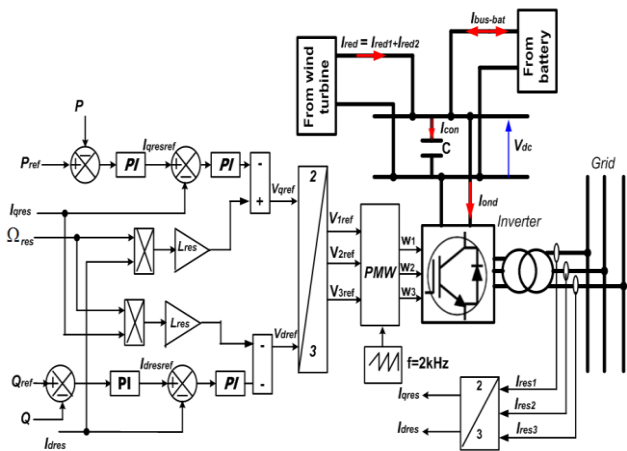


Fig.6. Active and reactive power control loops.

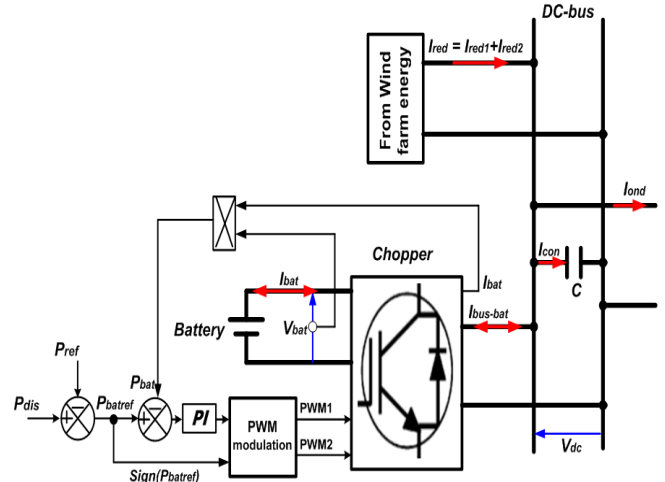


Fig.7. Battery's power control strategy.

$$\begin{cases} K_{pbat} = \sqrt{2} \cdot \omega_{nb} \cdot L_{bat} \\ K_{ibat} = \omega_{nb}^2 \cdot L_{bat} \end{cases} \quad (17)$$

3.4. DC-bus voltage control method

DC-bus voltage control strategy is illustrated in Fig.8, where the reference current in q axis I_{qref} is obtained from DC-bus voltage control loop. I_{dref} is fixed to zero to obtain a power factor of 1. Like to PMSG speed control, PI controller is used for DC-bus voltage management. The coefficients of this controller are expressed in (18), where ω_n and t_{sdc} are respectively the dynamics of the system, and system time constant.

$$\begin{cases} K_{pdc} = \sqrt{2} \cdot \omega_n \cdot C \\ K_{idc} = \omega_n^2 \cdot C \end{cases}, \omega_n = \frac{5.8}{t_{sdc}} \quad (18)$$

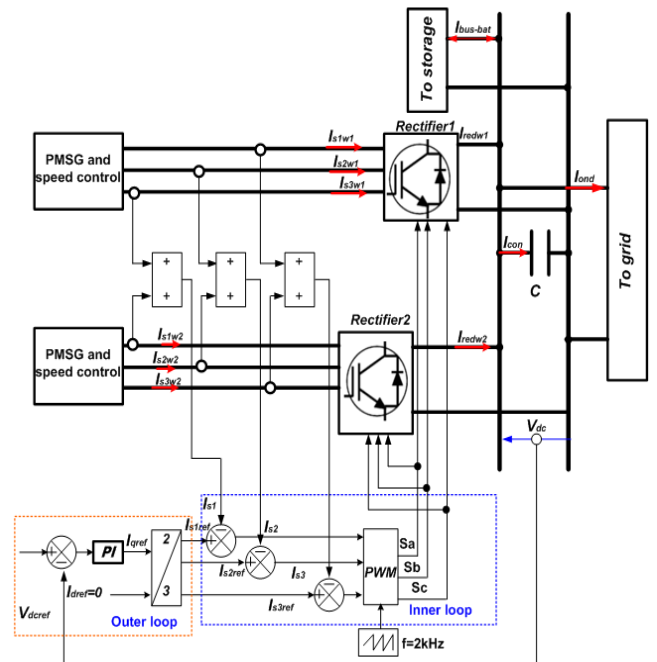


Fig.8. DC-bus voltage control strategy.

4. Simulation Results

For system simulations, the wind speed averages values are fixed to 11.4m/s, and used parameters are presented in Appendix section. DC-bus voltage reference is respectively fixed to 5kV and 6kV to show the performances of the control.

The active power profile requested by electrical grid manager [19] P_{ref} and available power from the wind farm P_{dis} are plotted in Fig.9. These curves are not same. To obtain the requested power profile by electrical grid manager using energy storage device is necessary. Fig.9 shows two main areas:

- The first situation is obtained if available power from wind farm P_{dis} is greater than requested P_{ref} . The difference between these ones must be assigned to energy storage device (battery).
- The second situation appear if available power from wind farm P_{dis} is less than requested power P_{ref} . In this case, the difference between these last ones must be supplied by energy storage device (battery).

Fig.10 shows the wind speed profiles for two wind turbines, the minimum and maximum values are respectively 10.75m / s and 12.5 m/s. These speeds are in the same direction but shifted of 73s, which correspond to ratio of distance between two turbines and average wind speed (11.4m/s). Used distance between two wind turbines is estimated as seven times of the turbine diameter (7x120=840m). The wind turbines speeds control results are presented in Fig.11 and Fig.12. These curves show that, the proposed control strategy is satisfactory, i.e. the controlled speeds are close to references estimated from (12).

The reference of active power is fixed by electrical grid manager which corresponds to P_{ref} . That of reactive power Q_{ref} is estimated using the active power reference as expressed in (19), where $tg(\varphi)$ is respectively fixed to 0.327; 0 and -0.327. These conditions are fixed from electrical “grid code” described in [20].

$$Q_{ref} = P_{ref} \cdot tg(\varphi), \begin{cases} tg(\varphi) = 0.327 \rightarrow Q_{ref} > 0 \\ tg(\varphi) = 0 \rightarrow Q_{ref} = 0 \\ tg(\varphi) = -0.327 \rightarrow Q_{ref} < 0 \end{cases} \quad (19)$$

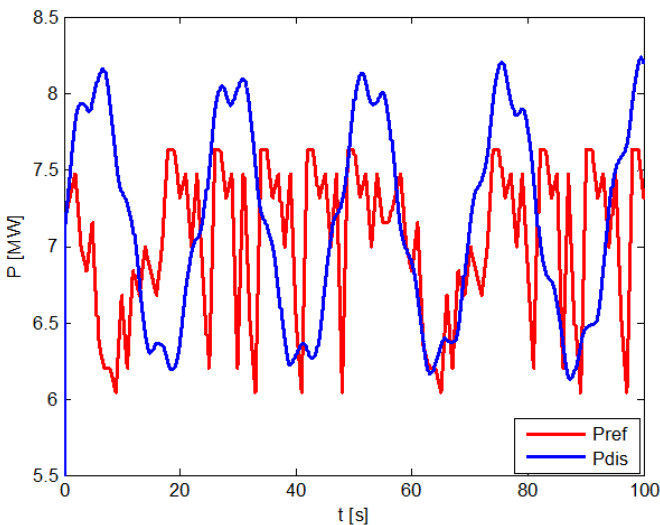


Fig.9. Requested power by electrical grid manager.

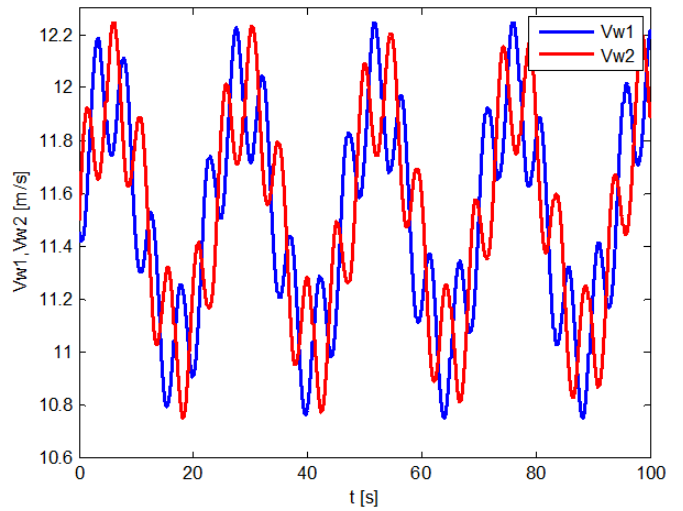


Fig.10. Wind speed profiles for two wind turbines.

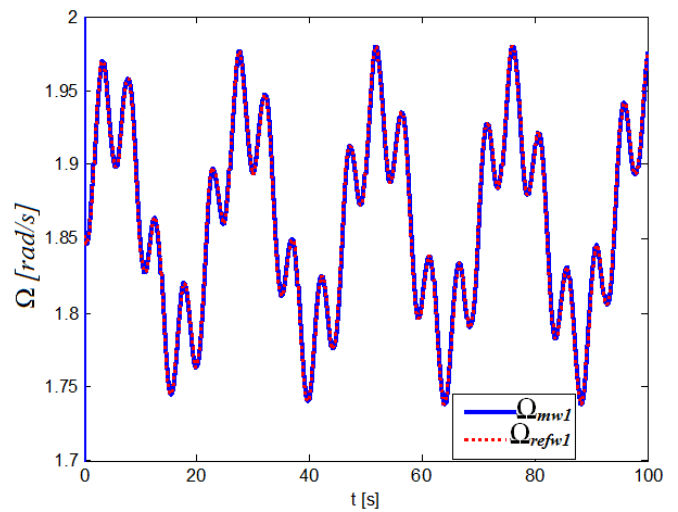


Fig.11. PMSG Speed control result for first wind turbine.

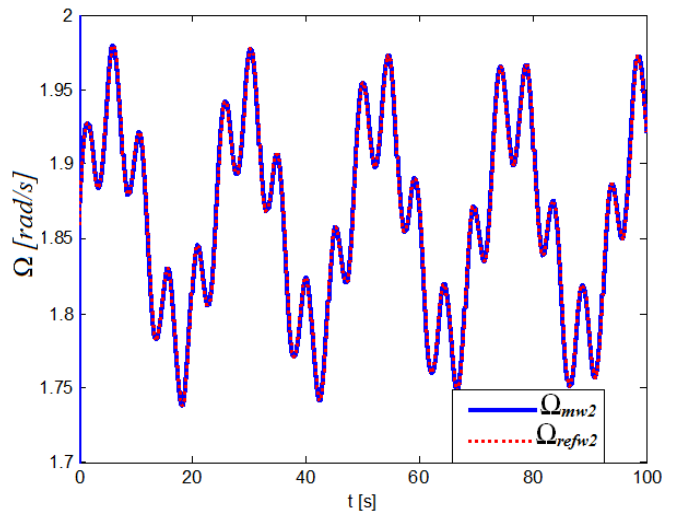


Fig.12. PMSG Speed control result for second wind turbine.

Active power control result is presented in Fig.13, where the required power for electrical grid P_{ref} is same to injected ones. Fig.14 shows the reactive power control result, the positive power corresponds to supplied power, and negative power for consumed power. These results allow concluding,

the proposed control strategies are satisfactory, and controlled powers are close to references ones.

The battery power control result is shown in Fig.15, where the reference is close to controlled power. In this figure, the positive power corresponds to the discharging operations and negative power corresponds to energy storage operations. This bidirectional operation allows compensate the wind energy fluctuations to obtain the required power for electrical grid. DC-bus voltage control result is presented in Fig.16. This curve shows that the DC-bus voltage follows the reference ones, which enables to conclude that the proposed control is adapted, except during initial conditions where DC-bus voltage control loop has not enough time to react.

Battery and wind farm contributions in DC-bus are presented in Fig.17. These curves show that, the injected current in inverter I_{ond} corresponds to sum of currents from two generators $I_{redw1}+I_{redw2}$ and that of the battery $I_{bus-bat}$, because DC-bus capacitor is charged during first operation. The positive parts of the current from battery pack correspond to energy supply operations and the negative parts correspond to energy storage operations.

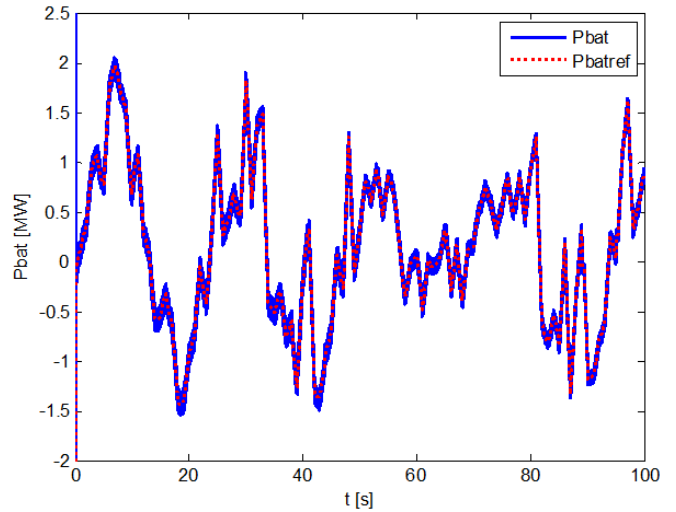


Fig.15. Battery's power control result.

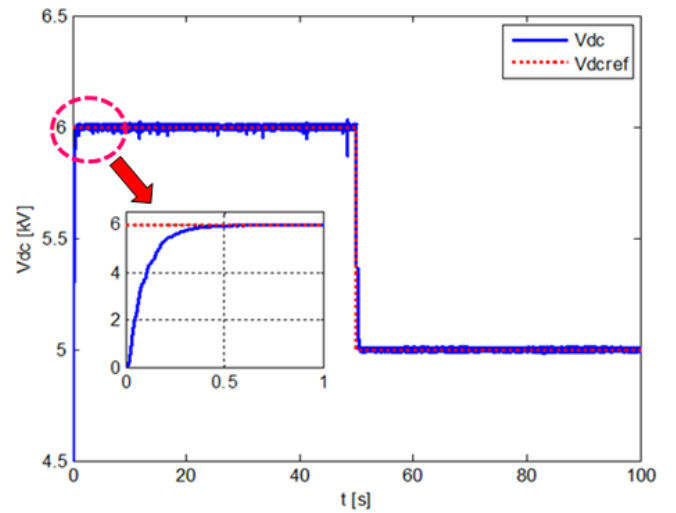


Fig.16. DC-bus voltage control result.

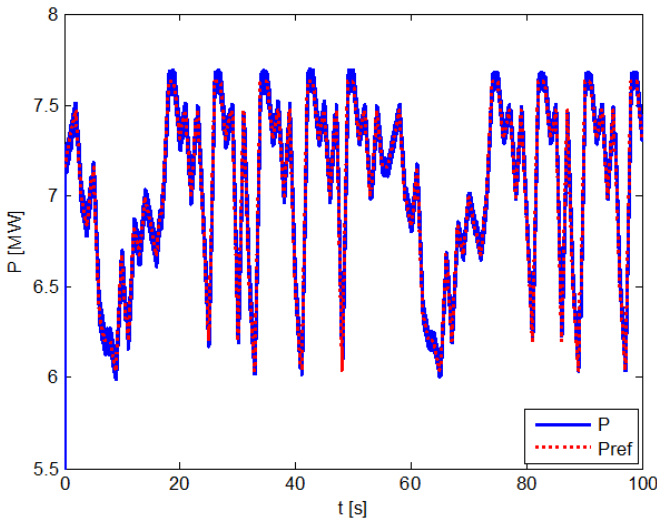


Fig.13. Active power control result.

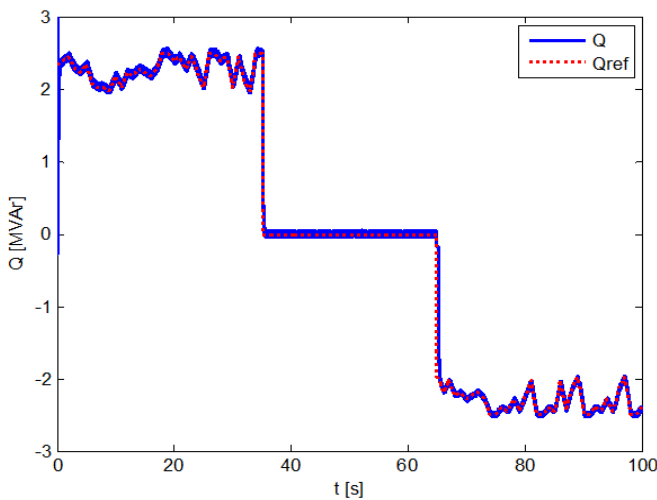
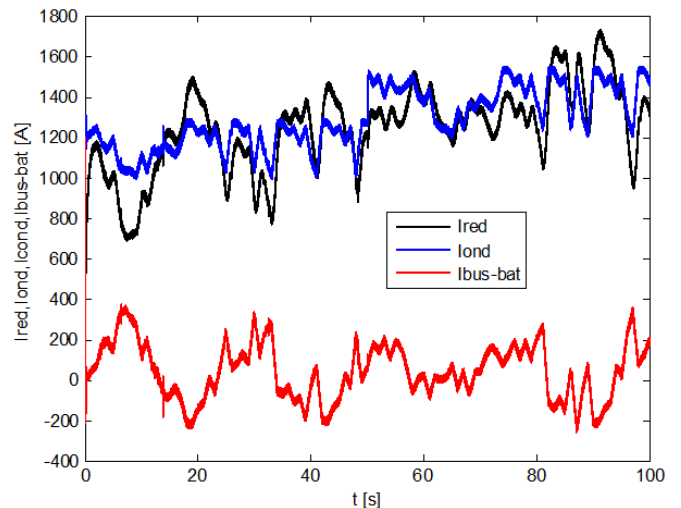


Fig.14. Reactive power control result.



Fi.17. Contributions of wind generators and battery in DC-bus.

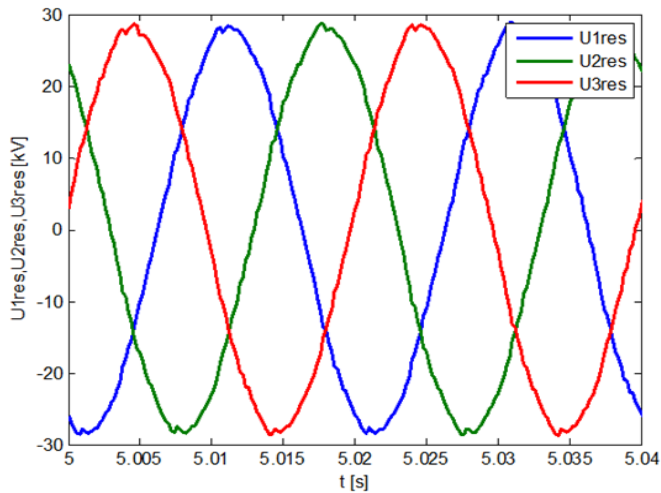


Fig.18. Phase to phase voltage of electrical grid in point of coupling.

Measured voltage on electrical grid in point of coupling is presented Fig.18, where the *RMS* voltage is not affected by injected reactive power due to performances of control.

5. Conclusion

In this paper, the authors present the modeling and control strategies of the wind farm based on Permanent Magnet Synchronous Generators connected to electrical grid and battery. Proposed control strategies are focused on generator’s speeds control, DC-bus voltage management, the active-reactive power control, and battery’s power management. The active/reactive power control strategy takes into account the required power profile for electrical grid due to battery’s contribution.

The simulation results show that, the proposed control strategies are satisfactory and the controlled variables are very close to references ones. Based on these simulations results, the PMSG and lithium-batteries seem to be interesting for offshore wind energy applications.

Appendix

Table 1. Permanent Magnet Synchronous Generator (PMSG) parameters

Parameters	Symbol	Values
PMSG rated power	P_n	5 MW
<i>RMS</i> voltage in stator	U_{sef}	3300 V
Resistance in stator	R_s	50 mΩ
Inductance in stator	L_s	7.5 mH
Number of pair of poles	P	60
PMSG inertia moment	J_m	2×10^5 kg.m ²
Induced magnetic flux	φ	28.6Wb

Table 2. Wind turbine parameters

Parameters	Symbol	Values
Wind turbine radius	R_t	60 m
Air density	ρ	1.225 kg/m ³
Optimal tip-speed ratio	λ_{opt}	9.7
Inertia moment of turbine	J_t	30×10^6 kg.m ²
Maximum power coefficient	C_{pmax}	0.53

Table 3. DC-bus and electrical grid parameters

Parameters	Symbol	Values
DC-bus voltage reference	V_{dcref}	6kV and 5kV
DC-bus capacitor	C	30mF
Electrical grid resistance	R_{res}	60 Ω
Electrical grid inductance	L_{res}	0.06H
Phase to phase <i>RMS</i> voltage for electrical grid	U_{res}	20 kV

Table 4. Lithium-battery parameters [21]

Parameters	Symbol	Values
Battery’s cell rated capacity		65Ahr
Open circuit voltage for one cell	E_{bat}	19.2V
One cell series resistance	R_{Ω}	0.00942 Ω
One cell polarization resistance	R_C	0.0736 Ω
Rated capacitance for one cell	C_C	4581F
Cells number in series	N_s	163
Cells number in parallel	N_p	56

References

- [1] M. Liserre and M. Molinas, “Overview of Multi-MW Wind Turbines and Wind Parks,” IEEE Trans. Ind. Electron., vol. 58, no. 4, pp. 1081–1095, 2011.
- [2] F. Spinato, P. Tavner, G. Bussel, and E. Koutoulakos, “Reliability of wind turbine subassemblies,” IET Renewable Power Generation, vol. 3, no. 4, p. 387, 2009.
- [3] C.E.A. Silva, D.S. Oliveira, L.H.S.C. Barreto, R.P.T. Bascopé, “A Novel Three-phase Rectifier with High Power Factor for Wind Energy Conversion Systems”, Power Electronics Conf., 2009, COBEP '09, pp. 985-992.
- [4] C. Sasi and G. Mohan, "Performance Analysis of Grid Connected Wind Energy Conversion System with a PMSG during Fault Conditions", International Journal of Engineering and Advanced Technology (IJEAT), ISSN: 2249 – 8958, Vol.2, no.4, April 2013.
- [5] T.H. Nguyen and D.C. Lee, "Advanced Fault Ride-Through Technique for PMSG Wind Turbine Systems Using Line-Side Converter as Statcom", IEEE transactions on industrial electronics, vol. 60, no. 7, pp.2842-2850, July 2013.
- [6] M.S. Camara, M.B. Camara, B. Dakyo and H.Gualous, “Modeling and Control of the Offshore wind energy system based on 5MW DFIG connected to grid”, IEEE-AFRICON, pp.991-995; Sept.2013.
- [7] B. Singh and S. Sharmay, “Stand-Alone Wind Energy Conversion System with An Asynchronous Generator,” Journal of Power Electronics, vol. 10, no. 5, pp. 538-547. Sept. 2010.
- [8] M.S. Camara, M.B.Camara, B. Dakyo, H. Gualous, “Modélisation et commande d’une génératrice synchrone à aimant permanent pour la production et l’injection des énergies offshore dans un réseau”, SGE2014, ENS Cachan, 8 - 10 juillet 2014

- [9] M. Coleman, W.G. Hurley, C. K. Lee, "An Improved Battery Characterization Method Using a Two-Pulse Load Test", IEEE Trans. on energy conversion, vol.23, no. 2, pp. 708-713, jun.2008.
- [10] L.R Chen, "Design of Duty-Varied Voltage Pulse Charger for Improving Li-Ion Battery-Charging Response", IEEE Trans. Industrial Electronics, vol.56, no. 2, pp. 480-487, Feb.2009.
- [11] S. Stockar, V. Marano, M. Canova, G. Rizzoni, L. Guzzella, "Energy-Optimal Control of Plug-in Hybrid Electric Vehicles for Real-World Driving Cycles", IEEE Trans. on Vehicular Technology, vol.60, no.7, pp. 2949- 2962, Sept.2011.
- [12] K. Murashko, J. Pyrhonen and L. Laurila, "Three-Dimensional Thermal Model of a Lithium Ion Battery for Hybrid Mobile Working Machines: Determination of the Model Parameters in a Pouch Cell" IEEE Transactions on Energy Conversion, Vol. 28, No. 2, June 2013.
- [13] H. He, R. Xiong and J. Fan, "Evaluation of Lithium-Ion Battery Equivalent Circuit Models for State of Charge Estimation by an Experimental Approach", Energies 2011, 4, 582-598.
- [14] A.M. Dhirde, N.V. Dale, H. Salehfar, M.D. Mann and T. H Han," Equivalent Electric Circuit Modeling and Performance Analysis of a PEM Fuel Cell Stack Using Impedance Spectroscopy",IEEE Trans. on energy conversion, vol. 25, no. 3, pp. 778-786, Sept.2010.
- [15] J.M. Corrêa, F.A. Farret, V.A. Popov, M.G. Simões, "Sensitivity Analysis of the Modeling Parameters Used in Simulation of Proton Exchange Membrane Fuel Cells", IEEE Trans. on Energy Conversion, vol. 20, no. 1, pp. 211-218, Mar.2005.
- [16] M.B. Camara, H. Gualous, F. Gustin, A. Berthon and B. Dakyo, "DC/DC converters design for Supercapacitors and Battery Power management in Hybrid Vehicle Applications-Polynomial Control Strategy", IEEE Transaction On Industrial Electronics, ISSN 0278-0046, Vol.57, No.2, pp. 587-597, February 2010.
- [17] D. Ikni, M.S. Camara, M.B. Camara, B. Dakyo and H. Gualous, "Permanent Magnet Synchronous Generators for Large Offshore Wind Farm Connected to Grid - Comparative Study between DC and AC Configurations", International Journal of Renewable Energy Research, Vol.4, No.2, 2014.
- [18] M.S. Camara, M.B. Camara, B. Dakyo and H. Gualous, "Permanent Magnet Synchronous Generators For Offshore Wind Energy System Linked To Grid - Modeling And Control Strategies", IEEE, 16th International Power Electronics and Motion Control Conference, PEMC2014, Antalya/Turkey, 21-24 September, 2014.
- [19] <http://siteelectrotechnique.free.fr/Documents%20GE1/doc%20production%20edf/prevconsoelec.pdf>
- [20] J. Aho, R. Jessler, A. Syomushkin and E. Catz, "Grid Code Compliance Support for Connecting Renewable Energy into Transmission Line using D-STATCOM System", CIGRE 2012.
- [21] M.B. Camara, B. Dakyo and H. Gualous, "Energy management based on Two-phase interleaved Buck-boost and Boost converters for Electric Vehicles Applications - Using Lithium-battery and Fuel cell", IEEE Inter. Conf. on Renewable Energy Research and Applications (IEEE-ICRERA 2012), 11-14 Nov. 2012, Nagasaki, Japan, Proceedings USB, ISBN: 978-1-4673-2328-4.